RSC Advances

ROYAL SOCIETY OF CHEMISTRY

PAPER

View Article Online
View Journal | View Issue

Check for updates

Cite this: *RSC Adv.*, 2025, **15**, 50734

Activating TiO_2 for visible light photocatalysis: a calcination approach to diesel photo-desulfurization under visible light

Asmaa S. Morshedy * and Aya M. Matloob*

Received 1st November 2025
Accepted 8th December 2025

DOI: 10.1039/d5ra08414h

rsc.li/rsc-advances

The increasing demand for clean fuels, coupled with stringent sulfur emission regulations, has driven the need for efficient and sustainable desulfurization technologies. In this study, a visible-light-active Black-TiO_2 by carbonization of Ti-MOF under vacuum was developed and evaluated for the photocatalytic desulfurization for sulfur-containing pollutant in diesel fuel that poses significant environmental risks. The White-TiO_2, Black-TiO_2, and Ti-MOF were synthesized through a simple method and comprehensively characterized using XRD, FT-IR, Raman spectroscopy, BET surface area analysis, SEM-mapping, UV-vis diffuse reflectance spectroscopy, and photoluminescence measurements. The Black-TiO_2 (Ti@C) demonstrated superior photocatalytic performance compared to individual W-TiO_2 or Ti-MOF catalysts, attributed to improved charge separation, reduced band gap, and strong interfacial interactions between Ti and C under visible light. Key operational parameters, including catalyst dosage, H_2O_2 concentration, and irradiation time, significantly influenced the degradation efficiency. Remarkable degradation efficiencies of 97.99% for real diesel feedstock (1300 ppm sulfur) for LHL, 99.53% under sunlight were achieved, with acetonitrile extraction effectively removing the oxidized sulfur compounds. The catalyst maintained excellent stability and reusability over six consecutive cycles, demonstrating its potential for practical fuel desulfurization applications. This research presents an environmentally friendly, a highly cost-effective, and energy-efficient approach to producing ultra-low sulfur fuels using solar energy.

1. Introduction

Demand for ultra-clean fuels has increased very significantly in recent years due to increasing environmental concerns and increasingly stringent world-wide emission standards. Air pollution, primarily driven by the combustion of fossil fuels, poses significant threats to human health and the environment. Sulfur compounds in fuels are major contributors to air pollution, leading to the formation of harmful emissions such as sulfur dioxide (SO_2), which can cause respiratory issues and acid rain. Addressing this challenge requires innovative approaches to reduce sulfur content in fuels effectively.[1,2] One of the most challenges in cleaner fuel production is the effective removal of sulfur-containing compounds from diesel fractions, which are known contributors to air pollution and acid rain when they are burned.[3,4] They also destroy catalysts in refining facilities, which become less effective and shorten their lifespan. So, it is necessary to remove sulfur from diesel to protect the environment, meet global fuel standards, and make the refining process more efficient.[5–9]

Diesel fuels typically consist of a broad spectrum of sulfur compounds such as mercaptans, sulfides, disulfides, thiophenes, benzothiophenes (BT), dibenzothiophenes (DBT), and their alkylated derivatives.[10,11] Conventional HDS technology, although good for lighter sulfur compounds, is high temperature (300–400 °C) and high pressure (3–5 MPa) with hydrogen supply, which is energy-consuming, expensive, and not environmentally friendly.[12,13] Besides, the existence of alkylated DBTs in diesel fuel results in incomplete sulfur removal, such that complementary or additional processes are required.[14,15] To address the limitations of hydrodesulfurization (HDS), oxidative desulfurization (ODS) has gained significant interest as a cost-effective alternative that operates under moderate conditions and offers high efficiency.[16,17]

Consequently, Photo-Oxidative Desulfurization (PODS) is seen as an advanced version of ODS, utilizing photocatalysts and visible light to enhance the oxidation rate. This approach benefits from renewable energy, the potential for free radiation sources, and low operating temperatures (ambient conditions).[18] This process (ODS) is performed at milder conditions than HDS and involves the oxidation of sulfur compounds into more polar sulfones or sulfoxides that can easily be extracted by using polar solvents.[19] Among the ODS processes, photocatalytic oxidative desulfurization (PODS) has been noted for its environmentally

---

Refining Department, Egyptian Petroleum Research Institute, Nasr City, Cairo, 11727, Egypt. E-mail: asma_2000asma@yahoo.com; Asmaa_Morshedy@epri.sci.eg; aya_mtloob@epri.sci.eg

benign process, involving light-activated catalysts to generate reactive oxygen species to selectively oxidize sulfur species. It can be carried out under room temperature and atmospheric pressure, and in some cases, even using natural sunlight.[20]

Several catalysts have been studied for the photocatalytic oxidation of sulfur compound such as zinc oxide,[21,22] graphitic carbon nitride,[23,24] cadmium sulfide,[25,26] molybdenum disulfide,[27,28] bismuth vanadate,[29,30] tungsten oxide,[31,32] metal–organic framework (MOF).[33–35]

Titanium oxide TiO_2 is the most commonly used material because of its abundant raw materials, simple preparation method and easy availability,[36] good chemical stability, environmental friendliness and high photocatalytic activity (a benchmark for research in the area of photocatalysis).[37] Also, have the advantage of high photo-reactivity, biological inertness and environmental friendliness.

TiO_2 has emerged as a leading photocatalyst in this field, known for its stability, non-toxicity, and strong oxidative capabilities. The photocatalytic activity of TiO_2 depends on its crystalline phase, anatase being the most active allotropic phase when compared to rutile and brookite.[38]

Although the wide diversity of approaches to utilizing TiO_2 is extremely diverse, spanning environmental applications (water purification, air pollution decomposition), medical applications (cancer therapy, anti-bacterial coating), energy-related technologies (hydrogen generation, CO_2 conversion and solar cells) and consumer products (self-cleaning surfaces), its application potential remains limited due to three fundamental challenges. The most significant limitation is its large bandgap (approximately 3.2 eV for anatase) that allows irradiation only to ultraviolet radiation, which accounts only for 5% of solar radiation, under-utilizing the abundant visible light (45%).[39] In addition, the photocatalytic activity can be seriously limited by rapid recombination of photogenerated (electron–hole) pairs with a reduction in quantum efficiency. Finally, the operation mode of photocatalysis requires continuous light illumination to maintain activity, thus this method cannot be commonly applied in low-light or dark conditions.[40]

Due to its electronic properties, TiO_2 suffers from low uptake of non-polar and hydrophobic contaminants as a result of its polar nature, as well being an inert surface due its non-porous structure.[41] In addition, the poor cycle reusability and recovery of nano-sized TiO_2 make it impractical for use in water solution, and poses a potential threat to both economy and environment.[42] In addition, the inherent agglomeration and aggregation of nanoparticles in such aqueous systems significantly reduces the effective surface area; thus impair light absorption and consequently reduce photocatalytic activity, but it is beyond our scope to delve further into their discussion.[43]

In order to overcome these intrinsic obstacles and increase the utilization efficiency of solar light, a great deal of interest is dedicated to the preparation of modified TiO_2 nanostructure.[44]

The calcination process is a critical step in the preparation of TiO_2, involving heating the material at high temperatures to enhance its structural integrity and photocatalytic performance. Calcination leads to improved crystallinity, increased surface area, and optimized electronic properties, all of which are crucial for maximizing photocatalytic activity. Additionally, TiO_2's band gap (3–3.2 eV) restricts its absorption to the UV range,[45] limiting its utility in broader applications. As a result, the development of effective visible-light photocatalysts is increasingly important to overcome these limitations.[46,47]

Titanium dioxide (TiO_2) doped with graphene (G) has garnered significant attention as a promising material for enhancing photocatalytic performance. TiO_2, while widely used for its strong photocatalytic activity, affordability, and stability, faces limitations such as rapid recombination of electron–hole pairs and restricted absorption in the UV range due to its wide band gap. Doping TiO_2 with graphene, a two-dimensional carbon material with high surface area, excellent conductivity, and remarkable electron mobility, addresses these challenges.[48] Graphene acts as an electron acceptor, reducing the recombination rate of photogenerated charge carriers and extending TiO_2's activity into the visible light spectrum. This synergistic effect between titanium dioxide (TiO_2) doped with activated carbon (AC) has emerged as a promising composite material in the field of photocatalysis.[49] While TiO_2 is widely recognized for its high photocatalytic activity, stability, and low cost, its performance is often limited by the rapid recombination of electron–hole pairs and its restricted absorption to the UV region due to a wide band gap. Doping TiO_2 with activated carbon, known for its high surface area, excellent adsorption properties, and ability to enhance charge separation, significantly improves its photocatalytic efficiency.[50] Activated carbon not only provides a larger surface area for pollutant adsorption but also acts as a conductive medium, facilitating better charge transfer and reducing electron–hole recombination. This combination leads to enhanced photocatalytic performance under both UV and visible light, making TiO_2/AC composites ideal for applications in water purification, air treatment, and pollutant degradation.[51]

In this context, metal–organic frameworks (MOFs) have garnered a lot of interest due to their strong catalytic potential, high surface area, and adjustable porosity.[52] Ti-MOFs, or titanium-based MOFs, are especially promising since they take advantage of titanium's photocatalytic activity. Their potential for photocatalytic applications has been increased by variations like black titanium and white titanium Ti-MOFs, which have shown unique optical and electrical characteristics. In order to promote photocatalytic activity under UV light, white titanium is usually composed of anatase TiO_2, which has a high bandgap energy and strong stability. Conversely, black titanium experiences hydrogenation or flaw engineering, which results in a reduced bandgap and improved visible light absorption. Because of these changes, black titanium is a flexible option for processes that rely on sunlight.[53]

This work will focus on the analysis of one specific synthesis modification strategy, calcination process, developed to tailor TiO_2 capable to utilize visible light and aimed at improved application of enhanced photo-desulfurization processes.

2. Experimental

2.1. Materials

1,4-Benzene dicarboxylic acid (H_2BDC, ≥98%), titanium isopropoxide (≥99.5%) and absolute ethanol (99.99%), were

Table 1 Characterizations and ASTM code for diesel feedstock

Characterization	Diesel feedstock	ASTM code
Yield, wt%	100	—
Refractive index, 20 °C	1.4669	D-1218
Density, 20 °C, g cm^{-3}	0.8268	D-1298
Sulfur content, ppm	1250	D-4294
Aniline point, °C	70.00 (158 °F)	D-611
Diesel index	52.15	—

obtained from Sigma-Aldrich Co., Ltd. Ammonium hydroxide solution (33%) was supplied by Merck in Germany. Hydrogen peroxide (H_2O_2, 30%) solution was also obtained from LOBA Chemie. Acetonitrile was provided by Sigma-Aldrich. Dibenzothiophene (DBT), silver nitrate ($AgNO_3$), benzoquinone (BQ), isopropanol (IPA), and ammonium oxalate (AO) were obtained from Sigma-Aldrich Co., Ltd. The petroleum diesel oil fraction was sourced from El-Nasr Petroleum Company. All materials were used as received, without any further treatment.

Diesel oil is a type of fuel that is commonly used for heating and industrial processes. It is also known by other names and synonyms such as heating oil, furnace oil, and kerosene oil. The diesel index is derived from the API gravity and aniline point (ASTM D611). The aniline point of any fuel is the lowest temperature, at which the fuel is completely miscible with an equal volume of aniline, where:

$$\text{Diesel index} = [\text{aniline point } (^{\circ}\text{F}) \times \text{API gravity}]/100 \quad (1)$$

Diesel index is a measure of the ignition quality of a diesel fuel. As the feedstock index increase, the ignition quality of the fuel will increase.[54,55]

2.1.1. Synthesis of Ti-MOF. In this study, Ti-MOF was synthesized through a solvothermal method.[56,57] Specifically, 0.004 mmol of titanium isopropoxide in water was combined with 0.0024 mmol of terephthalic acid (H_2BDC) in ethanol. The resulting solution was then placed into a Teflon-lined autoclave (V = 100 mL) and sealed within a stainless-steel vessel. The reactor underwent heating in an oven at 110 °C for duration of 24 hours, followed by a cooling period to room temperature. The white solid products obtained from the synthesized MOF were collected, washed multiple times with ethanol, and subsequently dried at 70 °C for duration of 12 hours.

2.1.2. Preparation of white-TiO_2 nanoparticles. In a typical synthetic procedure, Ti-MOF (1 g) was transferred to a muffle furnace, the furnace was quickly sealed and the mixture was calcinated at 500 °C for 3 h under oxygen atmosphere. Finally, the solid denoted as (W-TiO_2) was allowed to cool to room temperature.

2.1.3. Preparation of Ti@C nanoparticles (black-TiO_2). In a typical synthetic procedure, Ti-MOF (1 g) was transferred to a sintering boat, which had been previously placed in a vacuum tube furnace filled with N_2. The furnace was quickly sealed and the mixture was annealed at 500 °C for 3 h under N_2 atmosphere. Finally, the solid was allowed to cool to room temperature (B-TiO_2).

2.2. Characterizations

The X-ray diffraction patterns (XRD) of the samples were obtained at room temperature using Cu Kα irradiation (λ = 1.5406 Å) operating at 36 kV tube voltage and 20 mA tube current. Data was collected between 10° and 70° (2θ) with a 0.02° step size. The function groups of the prepared samples were investigated using Fourier transformer infrared spectroscopy (FT-IR). The analysis was conducted utilizing the ATI Mattson 1001 within the wavenumber range of 400–4000 cm^{-1}. The function group is measured a Fourier-transform infrared (FT-IR) spectrophotometer (Nicolet iS-10, USA). The structural characteristics of the produced materials were determined using X-ray powder diffraction (XRD) on an X'Pert PRO PANalytical equipment with a Ni filter (=0.15406 nm). Using a Quantachrome NOVA 2000, the surface characteristics of the produced materials were assessed. Raman spectra were detected using a BRUKER 110/S spectrometer in the range from 150–4000 cm^{-1}. The analyzed materials were degassed at 60 °C for six hours as a pre-treatment step. An energetic dispersive X-ray (EDX) unit-equipped scanning electron microscope (SEM) model Quanta-250 FEG, FEI, Netherlands was used to capture the morphologies of these samples. The generated structures' optical characteristics were assessed through the utilization of a spectrophotometer model V-570 from JASCO-Tokyo, Japan and ultraviolet-visible diffuse reflectance spectroscopy (UV-vis DRS). Their optical properties were further investigated by generating photoluminescence (PL) curves using a Japanese-made Spectrofluoro-photometer model JASCO FP-6500 (Table 1).

3. Results and discussion

3.1. XRD

X-ray diffraction analysis (XRD) of the prepared Ti-MOF, W-TiO_2, B-TiO_2, were studied and represented in Fig. 1. For Ti-MOF, it can be seen that Ti-MOF shows a strong diffraction peak at 2θ around 4.00° with a series broad diffraction peak at 2θ 18.50°, 29.80°, and 44.90°, which can be attributed to the successful synthesis of Ti-MOFs. The result agrees with the previous report.[58] The diffractogram of both B-TiO_2 and W-TiO_2

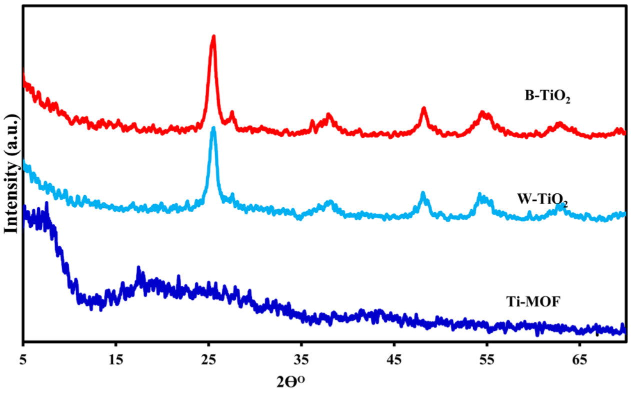

Fig. 1 XRD patterns of Black-TiO_2, Ti-MOF, and White-TiO_2.

catalysts show a huge and sharp peak at 25.2° indicates that there is a strong signal of (101) plane from anatase TiO_2, Other planes from anatase TiO_2 like (004), (200), (105) and (204) can be also seen in the pattern (PDF #86-1157).[59] Other than that, a small peak at 27.4° reveals that rutile phase also exists in W-Ti, and B-Ti, On the B-TiO_2, the intensity of rutile (110) plane becomes much higher than in the W-TiO_2, on comparing B-TiO_2 with W-TiO_2, it can be seen that position, intensity, and width of their XRD diffraction peaks are almost the same. This suggests that the Ti–O lattice of the B-TiO_2 sample did not change after low-temperature annealing.[60] The narrow XRD peaks and the absence of any additional impurity peaks suggest that as-prepared materials were successfully synthesized with high purity and good crystallinity.

3.2. FT-IR

Fourier transforms infrared spectroscopy (FT-IR) analysis of the prepared Ti-MOF, W-TiO_2 and B-TiO_2 samples were investigated at wavenumbers ranging from 4000 to 400 cm^{-1} (Fig. 2), to identify the functional groups on their surface and to provide complementary structural information to the X-ray diffraction results.

Fig. 2 shows FT-IR spectra of all the prepared titanium samples. FT-IR analysis exhibited standard characteristic bands and was employed to confirm the successful synthesis of Ti-MOF structure (Fig. 2): (1) the broad band at 3450 cm^{-1} assigned –OH groups,[61] indicates the presence of water molecules (2) bands at 1620 cm^{-1}, and 1480 cm^{-1} are corresponding to C=O and C–O group of carboxylic acid after coordination of H_3BTC to the metal center,[62] (3) the vibrational band at 1460–1100 cm^{-1} indicate (C=C) benzene rings that is present in the framework confirmed the successful synthesized of Ti-MOF. (4) The vibration bands appear around 450–700 cm^{-1} assigned O–Ti–O, (5) the vibrational stretching band at 620 cm^{-1} assigned Ti–O. For W-TiO_2 FT-IR spectrum shows the broad band at 3500 cm^{-1} corresponding to the stretching vibration the O–H bond, a band at 1620 cm^{-1}, corresponding to bending modes of water Ti–OH and characteristic bands of titanium dioxide are located at 450 cm^{-1} and 700 cm^{-1}.[63] For B-TiO_2 which carbonized at 500 °C in nitrogen, as shown from FT-IR spectra the very low intensity of organic ligand bands and the disappearance of –OH band which confirms the successful synthesis of B-TiO_2.

3.3. Raman spectroscopy

Raman spectroscopy has been used to confirm the structural features and the phase changes of the synthetic materials which include Ti-MOF, W-TiO_2, and B-TiO_2 which is depicted in Fig. 3. The synthesized titanium metal–organic framework showed characteristic vibrational signatures in the wavenumber region of 1450–1600 cm^{-1} due to aromatic rings C=C stretching along with peaks in the range of 470–730 cm^{-1} corresponding to Ti–O bond vibrations in the organic framework. These features support the successful synthesis of titanium metal organic framework which corresponds with the FT-IR results and previously reported scholarly papers.[64]

The W-TiO_2 obtained through the calcination of Ti-MOF in the presence of an oxygen atmosphere showed intense sharp Raman peaks at 145 cm^{-1} (E_g mode), 400 cm^{-1} (B_{1g}), 520 cm^{-1} (A_{1g}) and 640 cm^{-1} which identify the presence of anatase TiO_2. This clearly defined peak supports the claims of high crystallinity and purity of the anatase phase produced during oxidative activity which was also supported by the XRD results and scholarly documents. B-TiO_2, produced *via* calcination of Ti-MOF in nitrogen atmosphere showed less intense and broader peaks as compared to W-TiO_2. The E_g mode at 145 cm^{-1} was also broader and relatively shifted which means the presence of some oxygen vacancy and defect states.[65] These features of the structure undermine the synthesis attributed to the reductive atmosphere and are said to strengthen the absorption of visible light by lowering the bandgap energy of TiO_2.[66] This supports FT-IR organics data where ligand signals were less intense and –OH bands were mostly absent, confirming efficient carbonization.

Comparatively, these Raman results demonstrate the conversion of the Ti-MOF precursor into crystallized phases of TiO_2 with

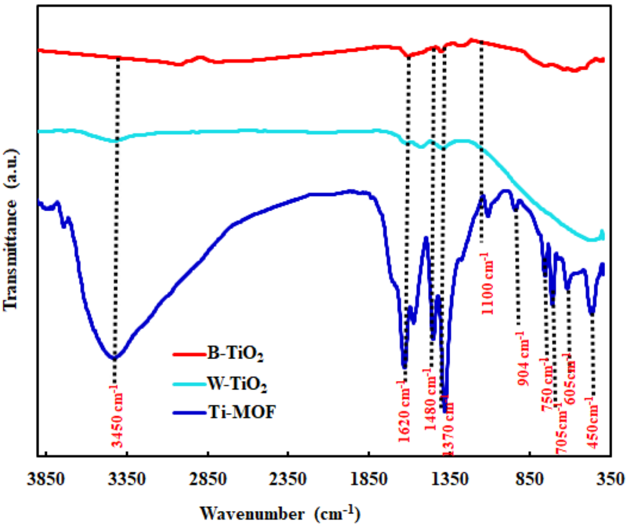

Fig. 2 FT-IR spectrum of Black-TiO_2, Ti-MOF, and White-TiO_2.

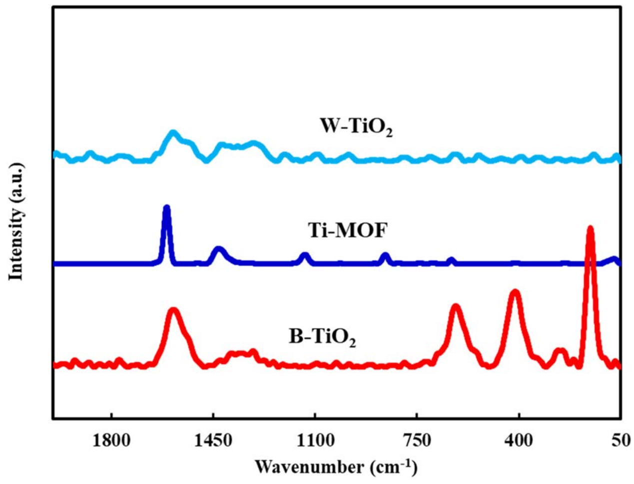

Fig. 3 Raman spectra of Black-TiO_2, Ti-MOF, and White-TiO_2.

distinguishing properties both optically and structurally. W-TiO_2 shows greater UV responsive crystallinity while B-TiO_2 thanks to its defect-rich structure has better visible-light responsiveness. These variances have a substantial impact on the efficiency of photocatalytic activity for oxidative desulfurization processes.

3.4. Scanning electron microscopy

Scanning electron microscopy shows distinct morphologic changes aligned with each material's photocatalytic capability. The parent Ti-MOF shows characteristic intergrown cubic crystallites (∼150 nm) along with edges and surface porosity reflective of its order, metallic–organic framework structure.[67] Fig. 4 shows the thermal transformation yields dramatically reconfigured architectures. B-TiO_2 reveals a mesoporous network of fused 30–80 nm nanoparticles with pronounced surface texturing which is enhanced light harvesting defect engineering.[66] In stark contrast, W-TiO_2 displays highly uniform spherical nanoparticles of 20 ± 5 nm with smooth crystalline faceted surfaces which means complete ligand burning and crystallization to the anatase phase.[68] These structural fingerprints directly reflect the materials' photocatalytic personas where B-TiO_2 with tortuous morphology boosts reactant adsorption and visible light activity, while geometrically perfect W-TiO_2 favors UV-driven quantum efficiency as shown in our photocatalytic tests (Section 3.7).

3.5. Transmission electron microscopy (TEM) analysis

TEM analysis was conducted to examine the internal morphology and nanoscale structure of the synthesized Ti-MOF, B-TiO_2, and W-TiO_2 materials (Fig. 5). The Ti-MOF sample displays crystalline domains intergrown into broad particles with cubic or rectangular shapes. The uniform particle morphology and internal porosity align well with the metal–organic framework structure assumed to be synthesized from the coordination of titanium isopropoxide with terephthalic acid. Such features depict that the MOF synthesis was successful, providing a scaffold-like structure template for oxide formation through thermal processing.[64]

B-TiO_2 was found to have a mesoporous fused nanoparticulate network with the individual particles being 30–80 nm in size after performing nitrogen chamber calcination. The particles appeared rough and porous suggesting surface defect formation due to carbonization. Such features corroborate findings on B-TiO_2 that incorporate defect engineering and carbon doping, resulting in enhanced absorption of visible light and photocatalytic activity.[66] The nanoporous network should also enhance surface area thereby increasing reactant adsorption; augmenting

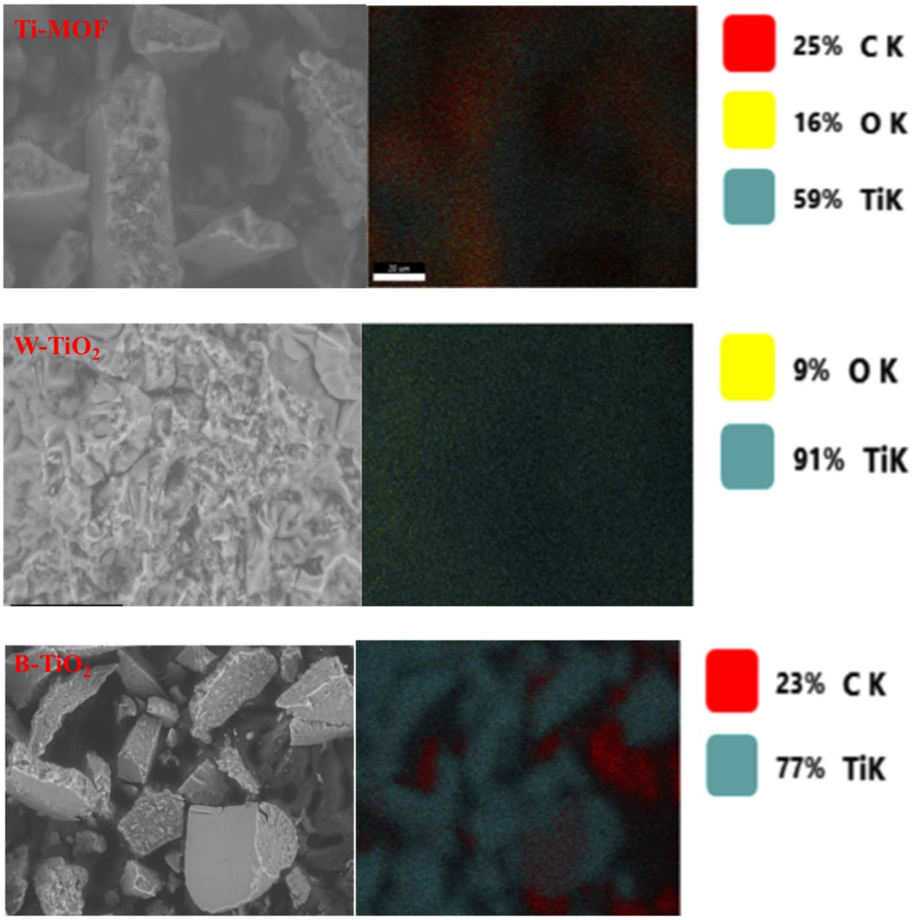

Fig. 4 SEM patterns of the Black-TiO_2, Ti-MOF, and White-TiO_2.

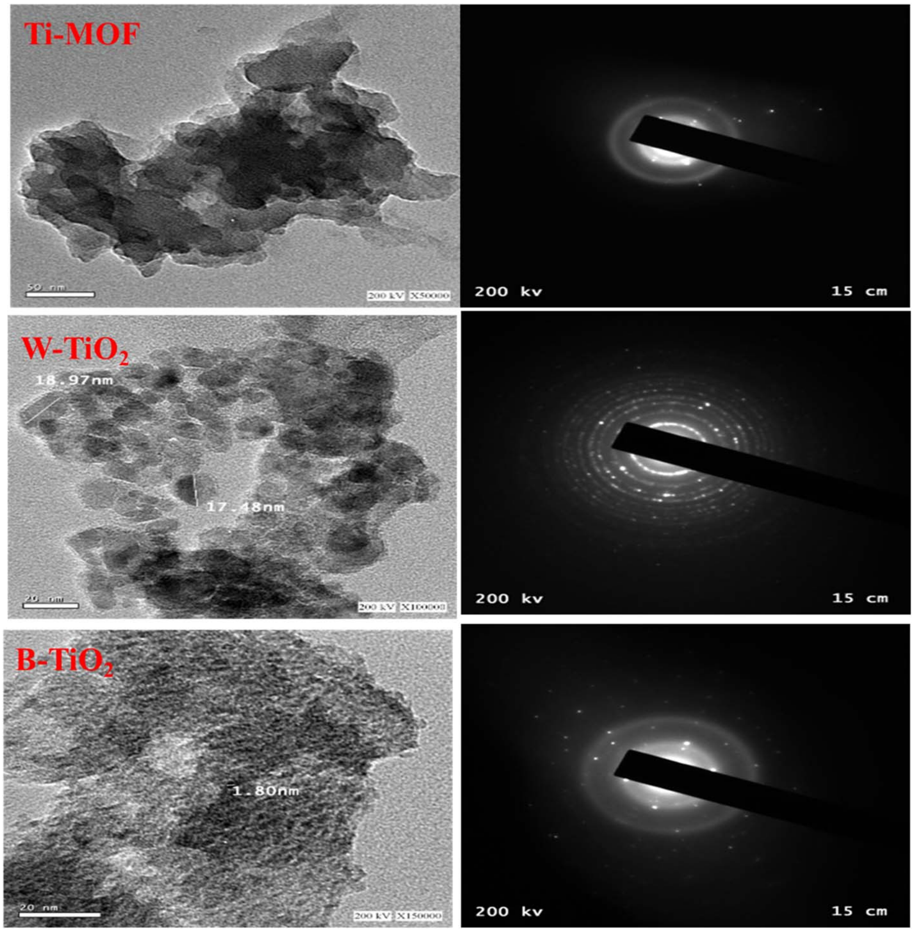

Fig. 5 HR-TEM patterns of the Black-TiO_2, Ti-MOF, and White-TiO_2.

photocatalytic sulfur removal. On the other hand, W-TiO_2 obtained *via* calcination in an oxygen atmosphere featured smooth spherical nanoparticles with a mean diameter of 20 ± 5 nm. These nanoparticles exhibited smooth surfaces and high crystallinity, which demonstrates complete transformation of the Ti-MOF precursor into anatase TiO_2. The absence of defects and irregularities implies a purer phase with low disorder, which is expected from a UV-active photocatalyst attributed to the predominant anatase phase.[68] These morphological distinctions between B-TiO_2 and W-TiO_2 underscore the influence of the thermal environment on structural evolution. While W-TiO_2 favors crystallinity and UV activity, B-TiO_2's defective structure enhances light harvesting under visible light, as corroborated by photocatalytic performance data discussed in Section 4.

3.6. X-ray photoelectron spectroscopy (XPS)

X-ray photoelectron spectroscopy (XPS) analysis is carried out to understand the nature of the functional groups present on the surface and the atomic percentage of elements of the prepared material. Survey spectra of B-TiO_2 contain: Ti 2p, C 1s, O 1s peaks are graphically illustrated in (Fig. 6a). Which confirm that the surface is composed mainly of titanium, oxygen, and carbon elements.

The high-resolution Ti 2p spectrum (Fig. 6b) displays two well-defined peaks located at approximately 458.5 eV and 464.2 eV, which correspond to Ti $2p_{3/2}$ and Ti $2p_{1/2}$, respectively. This spin–orbit splitting of ~5.7 eV is characteristic of Ti^{4+} in TiO_2, confirming that the titanium in the B-TiO_2 sample maintains the +4 oxidation state without noticeable reduction to lower oxidation states such as Ti^{3+}.

The O 1s spectrum (Fig. 6c) shows a wide peak at 530.0 eV for lattice oxygen (Ti–O–Ti). It is observed with a prominent shoulder at increased binding energy (~531.5–532.0 eV) that reveals the existence of surface hydroxyl groups and/or oxygen vacancies. These oxygen defects account for enhancing visible-light photocatalytic activity of B-TiO_2 as active sites and also promoting charge separation.

The C 1s spectrum (Fig. 6d) shows a dominant peak at 284.8 eV for C–C/C–H bonds, and weak peaks at higher binding energies (~286–289 eV) due to C–O and C=O groups. The resultant carbon species may be from trace organic ligands or partial carbonization of the MOF precursor during nitrogen calcination and form a Ti@C hybrid structure. Carbon introduction is the reason for improved electrical conductivity as well as light absorption in the visible region.[66]

Collectively, the XPS analysis confirms the successful formation of B-TiO_2 with Ti^{4+} as the dominant oxidation state, presence of

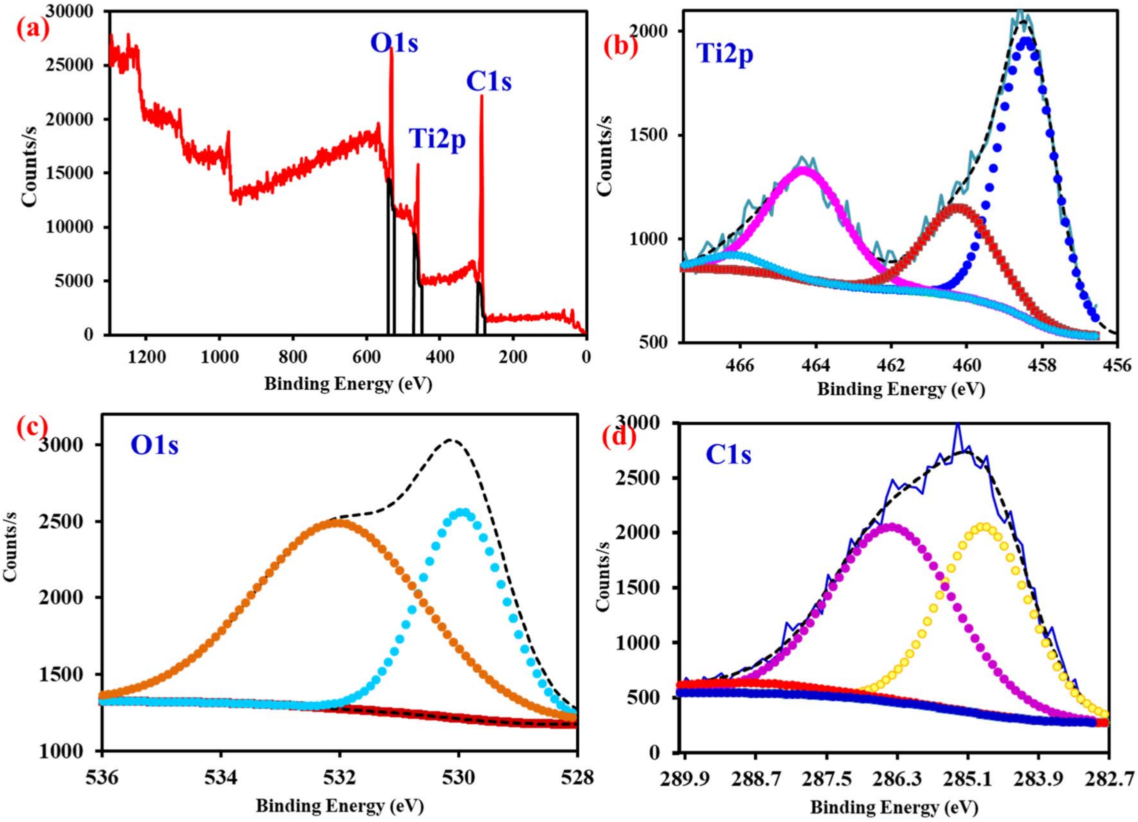

Fig. 6 XPS of the as-prepared Black-TiO_2, (a) survey, (b) Ti 2p, (c) O 1s and (d) C 1s spectra.

oxygen vacancies, and surface carbon, all of which are beneficial for enhancing photocatalytic activity under visible light irradiation.

3.7. Optical properties

The UV-vis diffuse reflectance spectra (DRS) presented in Fig. 7a reveal significant insights into the optical properties of the synthesized materials. The distinct reflectance peak at 450 nm for the B-TiO_2 sample suggests strong light absorption in the visible range, indicating its potential for applications in photocatalysis. In contrast, the peaks for W-TiO_2 and Ti-MOF at 370 nm and 380 nm, respectively, highlight their ability to absorb UV light, which may be advantageous for processes requiring high-energy photons. The UV-vis spectra indicate that the incorporation of carbon (carbonization) into the TiO_2 (through the calcination of the Ti-MOF in vacuum) exhibits a red significant absorption in the visible spectrum, with the absorption edge shifting to longer wavelengths, suggesting its potential for superior photocatalytic performance under visible light conditions.[69]

The band gap energies of the three samples were determined from their optical absorption spectra using Tauc's equation (eqn (2)):

$$(\alpha h\nu)^n = A(h\nu - E_g) \tag{2}$$

where α is the coefficient of absorption, $h\nu$ is photon energy, A is a constant, and E_g is the optical bandgap, respectively.

The calculated band gap values further enhance our understanding of these materials' electronic properties as presented in Fig. 7b. The band gap of 2.42 eV for B-TiO_2 (Ti@C) suggests a suitable energy threshold (facilitate enhanced charge carrier mobility) for visible light absorption, making it particularly relevant for solar energy conversion applications. This reduction in band gap enhances the materials' ability to absorb visible light, indicating their potential as effective photocatalysts for photo-desulfurization process. Meanwhile, the higher band gaps of W-TiO_2 (3.36 eV) and Ti-MOF (3.10 eV) imply that they are better suited for UV-driven processes, potentially limiting their utility in visible light applications. The characterization of these materials through UV-vis DRS and band gap analysis provides valuable information on their potential applications in photocatalysis, solar energy harvesting, and other fields requiring tailored optical properties. Future studies could explore the photocatalytic efficiency of these materials in various reactions, further validating their practical utility.

The charge migration and transfer performance of the as-synthesized samples were evaluated through photoluminescence (PL) spectra analysis. Generally, photocatalysts are designed and utilized to enhance photocatalytic efficiency by minimizing electron–hole recombination rate, as the rapid recombination of electrons and holes is a key limitation in photocatalysis. PL intensity is directly related to the recombination rate of photo-induced charge carriers, where higher PL

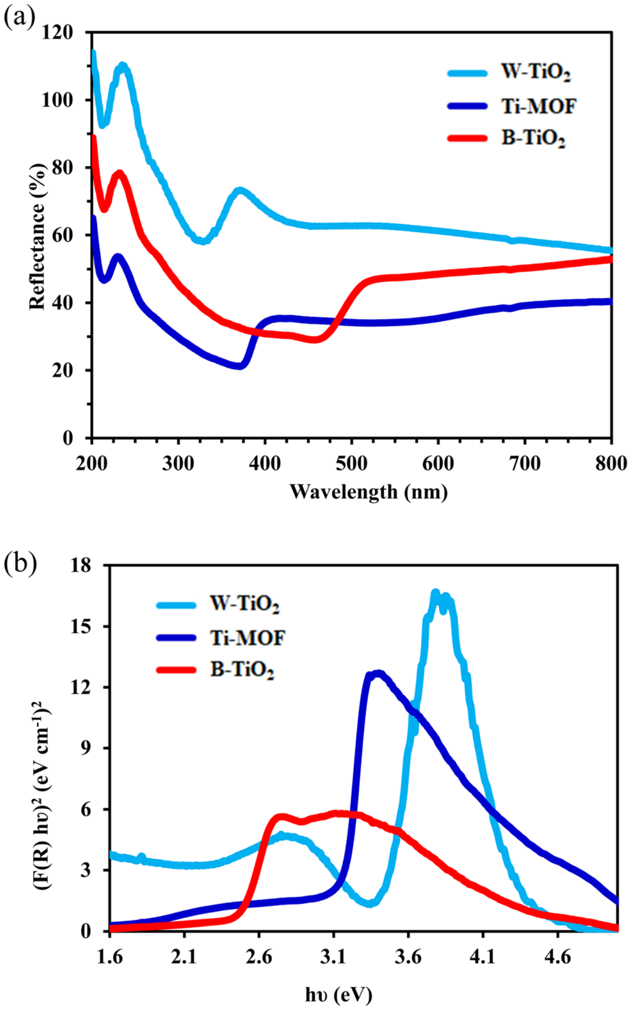

Fig. 7 (a) UV-visible reflectance of Black-TiO_2, Ti-MOF, and White-TiO_2. (b) Band-gap of the Black-TiO_2, Ti-MOF, and White-TiO_2.

intensity under light irradiation indicates a greater rate of electron–hole recombination.[70] The photoluminescence (PL) curves shown in Fig. 8 indicate that B-TiO_2 exhibits the lowest PL intensity. The observation that B-TiO_2 has the lowest PL intensity indicates that it effectively suppresses charge carrier recombination. In photocatalytic applications, lower PL intensity is often correlated with enhanced photocatalytic activity, as it suggests that more exciting (electron–hole pairs) are available for participating in the catalytic process rather than recombining.[70]

The order of PL intensities is as follows: B-TiO_2 < Ti-MOF < W-TiO_2. This emphasizes the superior performance of B-TiO_2 and it the highest photocatalytic activity for removing the sulfur compounds in this work. This trend can be interpreted in terms of structural and calcination procedure differences among the as-samples. The presence of specific activated carbon in B-TiO_2 sample may facilitate efficient charge separation, thereby enhancing its photocatalytic capabilities. In contrast, higher PL intensities observed in the other samples, such suggest that these materials may experience greater charge carrier recombination, which can limit their effectiveness in photocatalytic reactions. The strong performance of B-TiO_2 aligns with its favorable band gap of 2.42 eV, which allows it to absorb visible light effectively, thus driving photocatalytic reactions. Additionally, exploring the material's stability under prolonged light exposure and its performance in real-world scenarios will be crucial for assessing its practical viability. In practical terms, this means that B-TiO_2 could be more efficient in applications such as environmental remediation, where light-driven processes are essential.

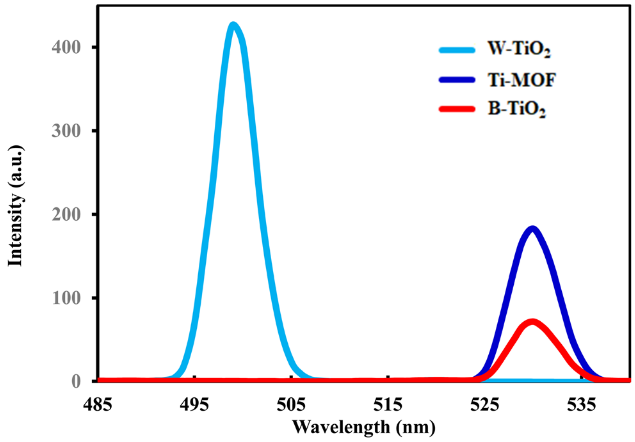

Fig. 8 PL spectroscopy of the Black-TiO_2, Ti-MOF, and White-TiO_2.

4. Photocatalytic activity of the prepared samples

During photocatalytic oxidative desulfurization experiments, linear halogen lamp with power 500 W (supplied by Orange-CT, USA) was used as the energy source. The photo-catalytic activity of the 1 gram of catalyst was studied for the degradation of sulfur compounds in the diesel oil (1300 ppm). In this experiment, 25 mL of feedstock and 0.1 g of the catalyst[69] were put to quartz-glass vessel connected with a reflux unit and set on the top of magnetic stirrer (500 rpm) inside a wooden box.[69] The experiments were carried out at different times. Different amounts of the catalyst. CH_3CN was investigated as solvent of extraction and H_2O_2 as an oxidizing agent. The used photocatalyst was separated by completion reaction time using the filtration technique. The sulfur content was determined utilizing an X-ray fluorescence (XRF), spectrophotometer model EDXRF SPECTROSCAN SL, USA. The study's focus on optimizing key operating parameters is particularly noteworthy. By fine-tuning the catalyst amount, time, and H_2O_2 to feed with solvent by two different ways, researchers were able to significantly enhance the photocatalytic activity. This level of optimization is critical for practical applications, as it allows for the development of tailored processes that maximize efficiency and minimize resource consumption. The ability to adjust these parameters to achieve optimal performance demonstrates the versatility of the developed photocatalysts.

4.1. Experiments in the dark and LHL light

Before conducting the photocatalytic process, the adsorption capacities of the as-synthesized catalysts for sulfur compounds

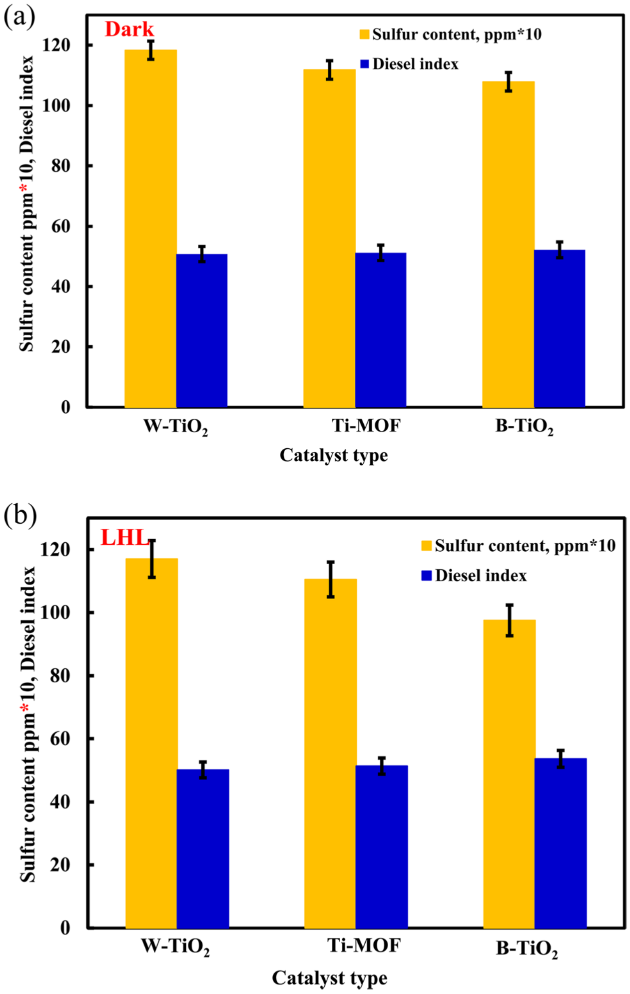

Fig. 9 (a) Effect of dark for Black-TiO_2, Ti-MOF, and White-TiO_2 for photo-desulfurization process. (b) Effect of LHL-light for Black-TiO_2, Ti-MOF, and White-TiO_2 for photo-desulfurization process.

were assessed under dark conditions over a 24-hour period. The results, illustrated in Fig. 9a, revealed that B-TiO_2, exhibited the highest adsorption performance, removing 17% of sulfur, compared to W-TiO_2 (9%) and Ti-MOF (14%), respectively.

Under visible light of (LHL, 550 nm, 500 watt, for 1 hour) the B-TiO_2 (Ti@C) displayed superior photocatalytic desulfurization efficiency, achieving 25% removal of sulfur compounds at a concentration of 1 g L^{-1}, Fig. 9b. This enhanced performance was attributed to its optimal band gap energy (2.42 eV) and improved charge carrier separation, as evidenced by earlier photoluminescence (PL) measurements (Fig. 8). The carbon within the B-TiO_2 (TiO_2@C) catalyst, derived from the controlled carbonization of the Ti-MOF precursor, plays several critical roles in enhancing photocatalytic performance. Firstly, it acts as a sensitizer, narrowing the band gap by introducing mid-gap states, which is directly responsible for the material's visible light absorption, as confirmed by UV-vis DRS. Secondly, the carbon serves as an excellent electron acceptor and conductor, facilitating the rapid separation of photogenerated electron–hole pairs and suppressing their recombination, a mechanism supported by our photoluminescence data. Finally, the integrated carbon framework contributes to the material's structural stability and provides a porous network that may enhance reactant adsorption. Therefore, the carbon is not a mere residue but an integral, functional component that enables the synergistic Ti–C interactions crucial for achieving high visible-light-driven desulfurization activity. Given these results, the B-TiO_2 was selected for further investigation into the effects of different operational parameters on the photocatalytic desulfurization of diesel feedstock (1300 ppm).

4.2. Effect of dosage of black-TiO_2

The effect of different dosages on the photocatalytic desulfurization was investigated as shown in Fig. 10. 25 mL of feedstock and 0.1–1.5 g of B-TiO_2 was introduced to photo-system for contact time 60 min under LHL light. The removal efficiency of DBT increased steadily with higher catalyst loading, reaching an optimum of 45% at 1 g L^{-1}. However, further increasing the catalyst concentration beyond 1.25 g L^{-1} led to a decline in activity, with removal dropping to 39%. This reduction in performance can be attributed to light scattering effects caused by excessive catalyst particles, which hinder effective photon absorption and reduce overall photocatalytic efficiency.[71]

4.3. Effect of oxidizing agent and solvent extraction technique

Another parameter investigated was the role of the oxidizing agent, H_2O_2, in the oxidation of sulfur compounds in diesel feedstock when combined with the B-TiO_2 photocatalyst. The experiments were conducted under optimal conditions (1 g L^{-1} catalyst dose, 1 hour irradiation under LHL). Fig. 11 demonstrates the influence of different addition of acetonitrile solvent (CH_3CN) with H_2O_2 addition methods on the photocatalytic desulfurization. The results revealed that feedstock without the catalyst shows limited removal while the presence of catalyst alone gives removal up to 45%. The addition of oxidant (H_2O_2) to the catalyst without any solvent shows a key role for the oxidation process for sulfur compounds, and the percent of sulfur removal slightly increase. In addition, Fig. 11 discuss the feedstock/H_2O_2/

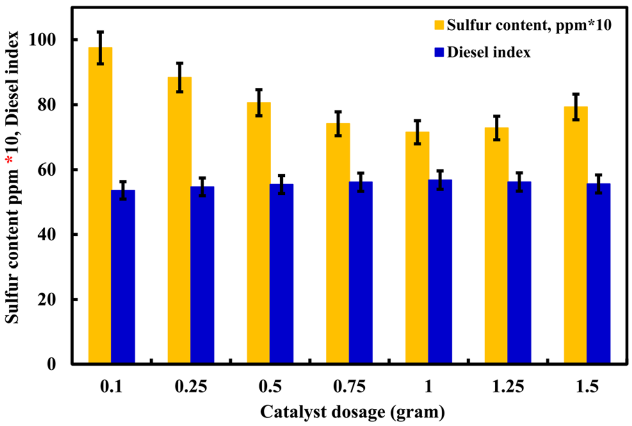

Fig. 10 Effect of dosage of Black-TiO_2 in photo-desulfurization process.

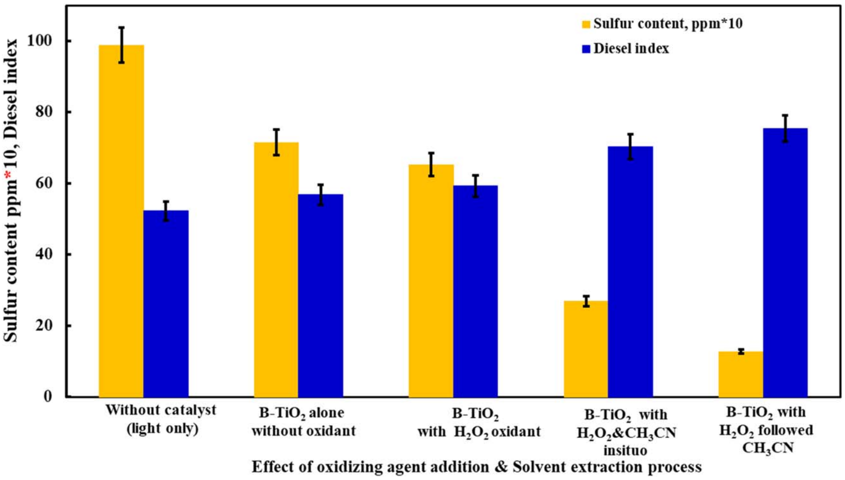

Fig. 11 Effect of oxidizing agent and solvent with Black-TiO_2 in photo-desulfurization process.

CH_3CN (*insituo*) yielded nearly 79.35% sulfur removal. These findings can be explained by presence of H_2O_2 led to increase the numbers of dissociated oxygen atoms.[72] As a result, elevated oxidation levels for sulfur compound are possible and can be easily removed. While a feedstock/H_2O_2 followed with CH_3CN (solvent extraction step) as a complementary step representing the highest efficiency achieved 90.22%, so this technique was chosen as a better technique for sulfur removal in this work, due to their high polarity, the previously oxidized sulfur compounds are strongly drawn to the solvent.[72] Also, Fig. 11 shows the diesel index of the produced diesel fuel was increased as sulfur content decrease and this is our big goal to obtain gasoil with low sulfur content and high diesel index. These findings highlight the potential of the B-TiO_2 photocatalyst as a highly effective and practical solution for photo-desulfurization process.

4.4. Effect of time

Following the optimization of catalyst type, dosage, and hydrogen peroxide addition, Fig. 12 presents the effect of contact time (15–90 minutes) on the desulfurization efficiency under these established conditions. The results demonstrate that maximum sulfur removal (97.99%) was achieved within 75 minutes. Notably, extending the reaction time beyond this optimal duration showed no significant improvement in the photo-desulfurization efficiency, suggesting that the process reaches completion within 75 minutes under the specified conditions.

4.5. Optimization the process under sunlight

The objective of this stage was to lower process expenses by substituting LHL with sunlight irradiation, using the previously determined optimal operating conditions, and testing them on real diesel fuel containing 1300 ppm sulfur. As reported by Morshedy *et al.*,[54] the average sunlight intensity in Egypt during the experiments was 1371 W m^{-2}. Under these optimal conditions, sulfur removal reached 99.53% with sunlight, surpassing the 97.99% achieved with artificial LHL (Fig. 13a). This stage also included a solvent extraction step using acetonitrile (CH_3CN) at a solvent-to-feed (S/F) ratio of 2 : 1 to eliminate oxidized sulfur compounds. From an economic and energy perspective, the desulfurization process employing B-TiO_2 photocatalyst proves to be a cost-effective method for producing ultra-clean diesel fuel.

4.6. Desulfurization kinetics

The kinetics of the dibenzothiophene (DBT) photocatalytic degradation process were evaluated using a pseudo-first-order kinetic model, with Fig. 13b provides critical insight into the degradation mechanism of dibenzothiophene (DBT) over the synthesized Black-TiO_2 photocatalyst, the analysis of which was conducted in accordance with the fundamental pseudo-first-order rate equation:

$$\log(q_e - q_t) = \log(q_e) - k_1 t/2.303 \tag{3}$$

where q_e and q_t are the adsorption capacities at equilibrium and time t, respectively, and k_1 is the rate constant.

The high linearity of the kinetic profile, confirmed by an R^2 value of 0.9997, substantiates the applicability of the pseudo-

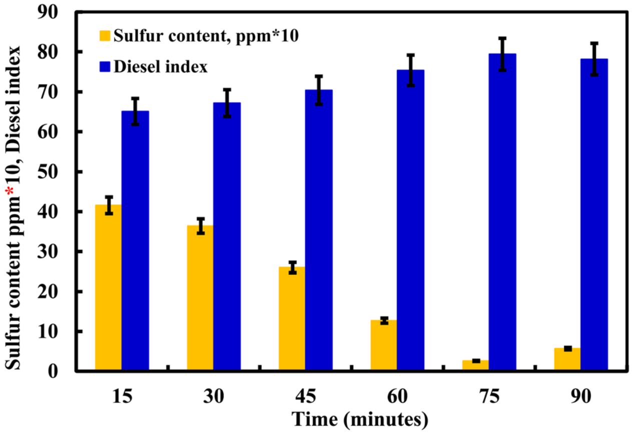

Fig. 12 Effect of time of Black-TiO_2 in photo-desulfurization process.

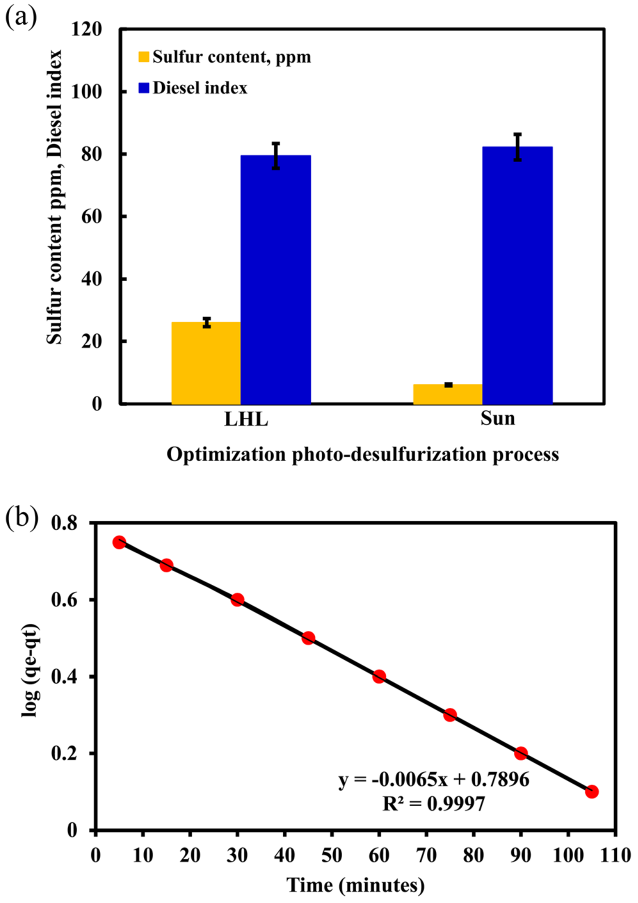

Fig. 13 (a) Optimization of Black-TiO_2 under sun-irradiation. (b) Pseudo-first-order kinetics of dibenzothiophene photo-degradation.

first-order model, indicating that the degradation rate is predominantly dependent on the concentration of DBT. Also, the high degree of linearity observed in the plot of $\log(q_e - q_t)$ *versus* time (t) strongly validates the applicability of this model, indicating that the rate-limiting step of the photocatalytic process is likely governed by the surface concentration of DBT molecules. The slope of this linear fit, calculated as $-k_1/2.302$, yields the apparent pseudo-first-order rate constant (k_1), which quantitatively describes the reaction velocity under the specified experimental conditions. A steeper negative slope would correspond to a higher k_1 value, signifying a more efficient photocatalytic system. Furthermore, the y-intercept of this plot provides an experimental value for $\log(q_e)$, allowing for the calculation of the theoretical pseudo-equilibrium capacity, which can be compared against the experimentally determined value to further assess the model's accuracy. The conformity of the experimental data to this kinetic model suggests that factors such as photon flux and catalyst mass were in sufficient excess, ensuring that the concentration of DBT was the primary variable controlling the degradation rate.[73] Therefore, Fig. 13b not only confirms the kinetic regime of the reaction but also serves as a fundamental tool for quantifying and comparing the photocatalytic efficiency of the Black-TiO_2 material.[45]

4.7. Reusability for the B-TiO_2 photocatalyst

The investigation of reusability for the B-TiO_2 catalyst is crucial for assessing their practical application in sustainable processes, such as desulfurization. The fact that B-TiO_2 was subjected to six cycles under optimal conditions demonstrates their potential for long-term use. The washing procedure, involving multiple rinses with toluene followed by ethanol, is important for removing residual reactants or byproducts that could hinder catalytic activity in subsequent cycles.

The observed decrease in sulfur removal efficiency after cycle 6 from 97.99% to 90.17% for B-TiO_2 (as showed in Fig. 14) provides valuable insights into the stability and durability of these catalysts. It demonstrates relatively better catalytic activity, which could be attributed to its structural integrity (Ti@C) or the effectiveness of its active sites in sustaining performance over multiple cycles. Also, the extraction capacity of the solvent used may be created and used repeatedly without losing its effectiveness; the approach offers a high long-term viability for practical applications.

These results also highlight the importance of catalyst calcination temperature and composition in achieving both high initial activity and stability over repeated use. Finally, the reusability tests underscore the potential of B-TiO_2 as a more stable option for sulfur removal, while also indicating the need for further investigation into the factors affecting catalyst longevity. These findings are essential for the development of effective and sustainable catalytic systems for environmental applications.

4.8. Spent B-TiO_2 photocatalyst

The structural and chemical integrity of the Black-TiO_2 photocatalyst was confirmed post-reaction through XRD and FT-IR analysis (Fig. 15a and b). The spectra for the spent catalyst remained largely unchanged compared to the fresh material, indicating excellent stability. However, the FT-IR analysis revealed the emergence of new vibrational modes at 1066 and 1122 cm^{-1}. The peak at 1122 cm^{-1} is assigned to oxidized sulfur compounds (SO_2) adsorbed on the TiO_2 surface, a phenomenon

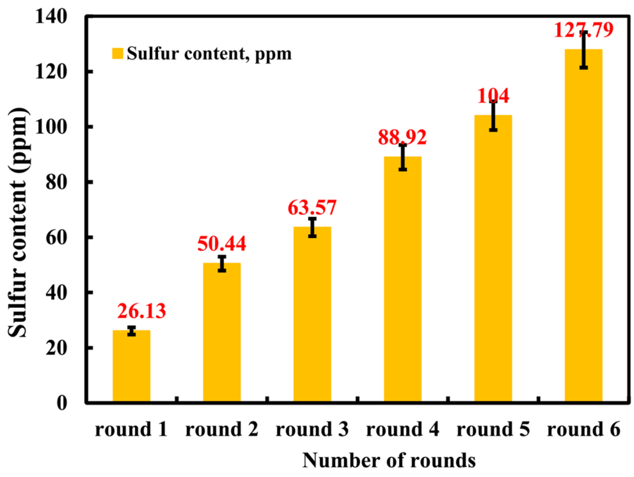

Fig. 14 Recyclability of Black-TiO_2 photocatalyst.

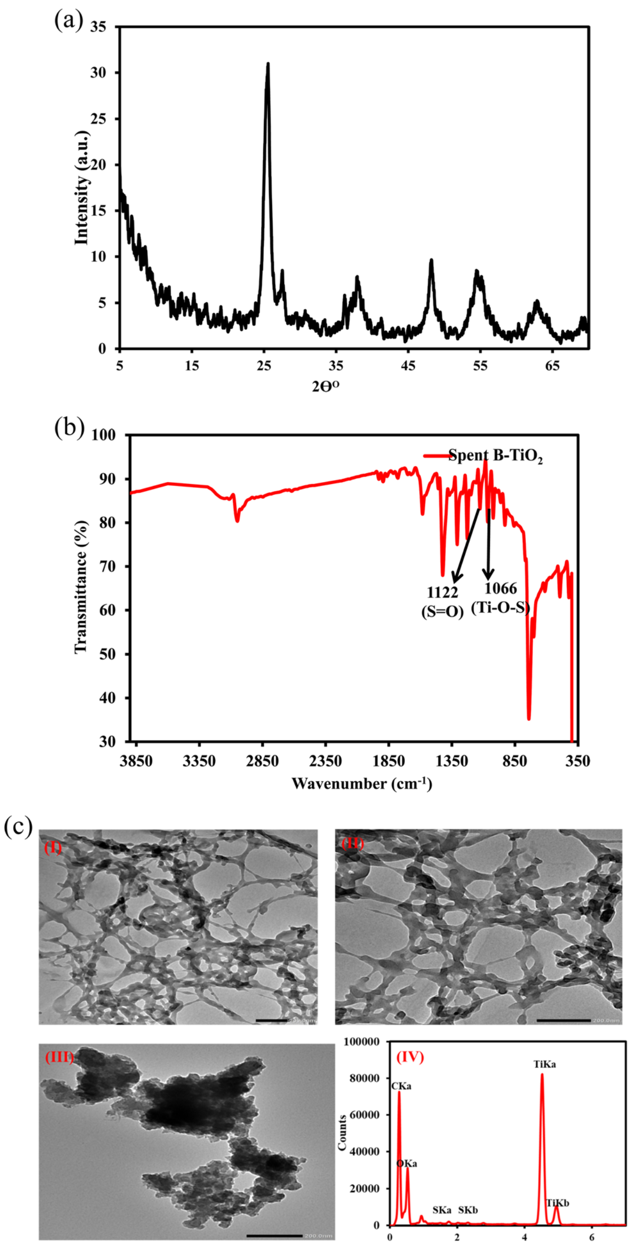

Fig. 15 (a) Spent XRD of Black-TiO$_2$ photocatalyst. (b) Spent FT-IR of Black-TiO$_2$ photocatalyst. (c) Spent TEM-EDX of Black-TiO$_2$ (Ti@C) photocatalyst.

that does not alter the solid's electronic structure.[74] In contrast, the peak at 1066 cm^{-1} arises from the stretching vibrations of Ti–O–S bonds,[74] providing direct evidence that sulfur compounds have been successfully incorporated into the TiO$_2$ lattice, leading to decrease the activity of the spent Black-TiO$_2$ photocatalyst after several rounds.

Complementing the spent XRD and FT-IR analyses, transmission electron microscopy (TEM) and energy-dispersive X-ray (EDX) spectroscopy provided further evidence of the catalyst's post-reaction state and the source of its deactivation. TEM micrographs (Fig. 15c) revealed a noticeable aggregation of spherical sulfur nanoparticles on the surface of the spent Black-TiO$_2$, indicating the deposition of byproducts from the diesel oxidation process. This visual observation was unequivocally confirmed by EDX spectroscopy, which detected distinct peaks corresponding to elemental sulfur (S). The presence of these sulfur deposits, both as adsorbed oxidized species and as aggregated elemental sulfur, physically blocks active sites on the photocatalyst surface and potentially impedes light absorption. This surface poisoning and light-shielding effect, rather than a collapse of the core TiO$_2$ structure, is identified as the primary mechanism for the observed decrease in photocatalytic activity after several reaction cycles.[45]

5. Mechanism of photo-desulfurization process

Fig. 16 illustrate the proposed mechanism for the photocatalytic desulfurization reaction discussed in this study. When the B-TiO$_2$, is exposed to LHL irradiation, the catalyst absorb photons,

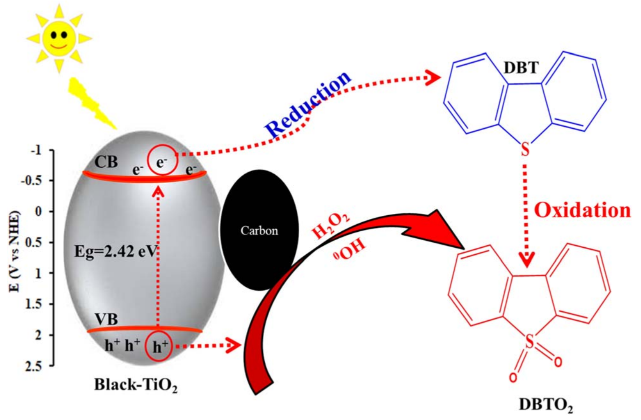

Fig. 16 Systematic diagram for the photocatalytic desulfurization process.

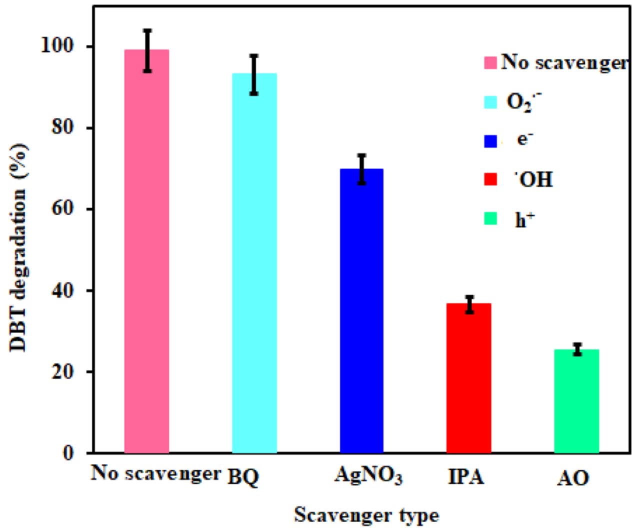

Fig. 17 Evaluation of reactive species roles *via* scavenger quenching experiments.

Table 2 Comparison of different catalysts for photo-desulfurization process

Photocatalyst	Conditions	Sulfur removal, %	Ref.
Ag–TiO_2 nanocomposite	DBT in model fuel; UV light (365 nm), H_2O_2	93–95	78
Cu–ZnO/TiO_2	Dibenzothiophene (DBT), (BT), (T), model fuel in *n*-hexane solvent (500 ppm), oxidant: H_2O_2 (30%), light source: 500 W Xe-lamp	88.12	79
Ag@AgBr/Al-SBA-15 derived from natural halloysite	Dibenzothiophene (500 ppm), 50 mg of the catalyst dosage, 1.0 mL of H_2O_2, for 360 min of sunlight irradiation at 70 °C	98.66	80
Cu-doped TiO_2/$BiVO_4$	DBT in model fuel; H_2O_2; visible light >500 nm	93	81
Au–m-TiO_2/g-C_3N_4	Dibenzothiophene (DBT), model fuel in *n*-octane (500 ppm), oxidant: H_2O_2, visible light >400 nm	98.7	82
$CoFe_2O_4$ nano-particles	DBT, 60 min at 40 °C under the conditions: 6 mL of model oil (600 ppm), O/S = 3 : 1 and 125 mg catalyst	95	83
Ultrasonically synthesized TiO_2	Thiophene, oxidant: H_2O_2, UV light	43 (toluene); 100 (*n*-hexane, *n*-octane)	84
Amorphous TiO_2 in ionic liquid	DBT, BT, 4,6-DMDBT, RSH, oxidant: H_2O_2, UV light, optimal reaction conditions	96.6	85
$H_5PV_2Mo_{10}O_{40}/TiO_2$	4-Methyldibenzothiophene (4-MDBT), oxidant: H_2O_2, temperature: 60 °C, UV light	99.0	86
HY@TiO_2-1.5	DBT, BT, oxidant: H_2O_2, temperature: 70 °C, UV light	99.7 for DBT, 85.0 for BT	87
Cu-impregnated carbon-doped TiO_2	0.1 mL H_2O_2, solvent to fuel ratio of 1, catalyst dosage of 2 g L^{-1}, and initial DBT (250 ppm)	98.27	88
Tl-doped TiO_2 nanofibers	Diesel fuel, oxidant: H_2O_2, light source: Xe lamp	98.74	69
TiO_2 in ionic liquid	Model oil and actual diesel oil, respectively, in 10 h UV irradiation under the conditions that V(IL)/V(oil) = 1 : 5, air flow = 200 mL min^{-1}	98.2 (model oil) and 94.3% (actual diesel oil)	89
Ti@C (Black-TiO_2)	Diesel fuel (1300 ppm), oxidant: H_2O_2, CH_3CN, light source: (LHL lamp, sun)	97.99 (LHL) and 99.53 (sun)	This work

leading to the excitation of their electrons. This excitation facilitates the transfer of electrons from the highest occupied molecular orbital (HOMO) to the lowest unoccupied molecular orbital (LUMO) edges of the structures, generating a significant number of electron–hole pairs. As B-TiO_2 is excited, photogenerated electrons transition from the valence band (VB) to the conduction band (CB), resulting in the creation of new electron–hole pairs.

The formation of electron–hole pairs during the excitation of B-TiO_2 is particularly noteworthy, as these pairs can participate in redox reactions that lead to the breakdown of sulfur-containing compounds. The migration of photogenerated electrons from the valence band to the conduction band of as B-TiO_2 underscores the efficiency of the material in harnessing light energy for catalysis. After certain time, the recombination of (electrons–holes) pairs in B-TiO_2 occur.

$$\text{Ti@C} + h\nu \rightarrow (\text{hole}^+) + (\text{electron}^-) \tag{4}$$

$$\text{Ti@C(h}^+) + \text{sulfur} \rightarrow \text{Ti@C} + \text{oxidation product} \tag{5}$$

$$H_2O_2 + h\nu \rightarrow 2^{\bullet}OH \tag{6}$$

$$\text{Ti@C(e}^-) + H_2O_2 \rightarrow 2^{\bullet}OH \tag{7}$$

$$2^{\bullet}OH + \text{sulfur compounds} \rightarrow CO_2 + H_2O + SO_4^{2-} \tag{8}$$

Since TiO_2 is an n-type semiconductor,[75,76] the B-TiO_2 (Ti@C) forms synergistic heterojunction, which plays a crucial role in the separation and transport of photoexcited charge carriers. This heterojunction effectively minimizes recombination losses while enhancing charge transfer efficiency, significantly boosting the composite's photocatalytic performance. Such properties highlight its strong potential for advanced photocatalytic applications in the future.[77] This is critical, as recombination can significantly diminish the photocatalytic efficiency by reducing the availability of active species necessary for sulfur removal. Overall, this proposed mechanism illustrates the complexity of photocatalytic reactions and the importance of material composition in optimizing performance. Future research could focus on quantifying the efficiencies of the catalyst, exploring the impact of varying the calcination temperature during the preparation process, and studying the influence of reaction conditions on the photocatalytic activity. Additionally, advanced characterization techniques could provide deeper insights into the electronic structure changes occurring during the photocatalytic cycle.

5.1. Trapping and identification of reactive photocatalytic species

To elucidate the contribution of key reactive species in the photodesulfurization mechanism, radical trapping experiments were conducted using specific chemical scavengers. The concentration of DBT after each test is measured on the UV-spectrophotometer model V-570 manufactured by JASCO (Japan). Silver nitrate ($AgNO_3$), benzoquinone (BQ), isopropanol (IPA), and ammonium oxalate (AO) were employed to selectively quench electrons (e^-), superoxide radicals ($O_2^{\bullet-}$), hydroxyl radicals ($^{\bullet}OH$), and holes (h^+), respectively, as further illustrated in Fig. 17. The radical trapping experiments revealed that the introduction of ($AgNO_3$), (IPA), and (AO), significantly suppressed the photocatalytic desulfurization of dibenzothiophene (DBT, 200 ppm), reducing the efficiency from 98.88% to 69.7%, 36.5%, and 25.4%, respectively. This pronounced quenching effect unequivocally identifies holes radicals (h^+) as the predominant reactive species governing the reaction. Also, IPA suggests that hydroxyl radicals ($^{\bullet}OH$) assume a secondary role in the photocatalytic mechanism. Based on this investigation the contribution of active species to the photocatalytic desulfurization of the DBT follows the order: $h^+ > {}^{\bullet}OH > e^- > O_2^{\bullet-}$.[70]

5.2. Comparative assessment of photocatalytic desulfurization efficiencies of black-TiO_2 photocatalyst *versus* other from recent publications

Photocatalytic desulfurization is an emerging field where numerous catalysts are being developed to harness solar energy effectively. Table 2 presents a comparative analysis of various catalysts, light sources, and sulfur removal efficiencies. In this study, the (B-TiO_2) catalyst demonstrated exceptional performance, achieving up to 99% removal of a 1300 ppm sulfur compounds of diesel feedstock under LHL irradiation (550 nm, 500 W). Remarkably, under natural sunlight, the sulfur removal efficiency exceeded 98% for real diesel feedstock. These results surpass those of other advanced catalysts, providing a strong basis for future research into the design and optimization of similar nanocomposite systems to further enhance photocatalytic desulfurization performance.

6. Conclusions

This innovative study has successfully highlighted the effect of calcination process for designing a photocatalyst for visible light-irradiation for desulfurization of gas oil feedstock (1300 ppm). The unique effects resulting to the creation of highly efficient and versatile photocatalytic systems. B-TiO_2 catalyst enhanced light absorption, promoted effective charge separation, and optimized interfacial charge transfer processes, which are essential for the efficient photocatalytic degradation of sulfur-containing compounds. This work developes a visible-light-active Black-TiO_2 *via* carbonization of Ti-MOF under vacuum with exceptional photocatalytic efficiency in photo-desulfurization of real sample diesel fuel (1300 ppm). The structural and optical properties of the three catalysts were thoroughly characterized using XRD, SEM-mapping, FTIR, Raman spectroscopy, XPS, UV reflectance, and photoluminescence spectra. Among the tested photocatalysts, the B-TiO_2 (Ti@C) exhibited the lowest photoluminescence (PL) recombination rate and the highest catalytic activity under visible light (500 W halogen lamp, 550 nm). The enhanced performance compared to W-TiO_2 or Ti-MOF was attributed to improved charge separation, synergistic interfacial effects, and superior visible-light absorption. Optimizing key operational parameters such as the catalyst amount, time, H_2O_2 and CH_3CN to feed ratio *insituo*, and separated step respectively, improved the desulfurization capabilities of the B-TiO_2 photocatalyst. Based on the active species trapping experiments, a feasible Z-scheme photocatalytic mechanism is proposed, confirming that superoxide radicals ($^{\bullet}O_2^-$) and holes (h^+) are the predominant active species in the photocatalytic oxidation desulfurization process. Furthermore, the fabricated flower-like AgI/Bi_2O_3 photocatalyst in this work demonstrates superior photocatalytic performance under visible light irradiation when compared to other reported AgI/Bi_2O_3 compounds.

Under optimized conditions, sulfur removal reached 97.99% (LHL) with diesel index 79.40 and 99.53% (sunlight) with diesel index 82.2, with acetonitrile extraction used to remove oxidized sulfur compounds (more polarized). The catalyst also demonstrated outstanding stability and reusability over six cycles, highlighting its practical potential. The reduction of sulfur compounds in fuels is essential for minimizing environmental pollutants and meeting regulatory standards. Moreover, the ability to operate under mild visible light and real sunlight aligns with the growing interest in using renewable energy sources for industrial processes. This work offers an eco-friendly, cost-effective, and sustainable solar-driven method for producing ultra-low-sulfur fuels, contributing to cleaner energy solutions.

Author contributions

Asmaa S. Morshedy: resources, methodology, investigation, formal analysis, data curation, conceptualization, software, validation, visualization, writing – original draft, writing – review and editing. Aya M. Matloob: resources, methodology, formal analysis, conceptualization, data curation, investigation, software, validation, visualization, writing – original draft, writing – review, and editing.

Conflicts of interest

The author reported no potential conflict of interest.

Data availability

All data is available in the manuscript and is available when requested by the corresponding author, asma_2000asma@yahoo.com (Asmaa S. Morshedy).

References

1 R. van den Hoed, Sources of radical technological innovation: the emergence of fuel cell technology in the automotive industry, *J. Cleaner Prod.*, 2007, **15**(11), 1014–1021.

2 T. Ryan and R. R. Maly, Fuel Effects on Engine Combustion and Emissions, in *Flow and Combustion in Reciprocating Engines*, ed. C. Arcoumanis and T. Kamimoto, Springer Berlin Heidelberg, Berlin, Heidelberg, 2009, pp. 381–420.

3 G. Corro, Sulfur impact on diesel emission control – A review, *React. Kinet. Catal. Lett.*, 2002, **75**(1), 89–106.

4 E. A. Oke, Examining the Effectiveness of Deep Eutectic Solvents in Removal of Sulfur from Fuel Oil: A Mini Review, *Chem. Afr.*, 2024, **7**(7), 3565–3578.

5 P. Saiyasitpanich, *et al.*, The Effect of Diesel Fuel Sulfur Content on Particulate Matter Emissions for a Nonroad Diesel Generator, *J. Air Waste Manage. Assoc.*, 2005, **55**(7), 993–998.

6 C. Song, An overview of new approaches to deep desulfurization for ultra-clean gasoline, diesel fuel and jet fuel, *Catal. Today*, 2003, **86**(1), 211–263.

7 E. Furimsky, Spent refinery catalysts: Environment, safety and utilization, *Catal. Today*, 1996, **30**(4), 223–286.

8 M. A. Alabdullah, *et al.*, A Viewpoint on the Refinery of the Future: Catalyst and Process Challenges, *ACS Catal.*, 2020, **10**(15), 8131–8140.

9 D. K. Chauhan, *et al.*, A two in one approach: renewable support and enhanced catalysis for sweetening using chicken feather bound cobalt(II) phthalocyanine under alkali free environment, *RSC Adv.*, 2016, **6**(57), 51983–51988.

10 D. K. Chauhan, *et al.*, Kinetics and feasibility studies of thiol oxidation using magnetically separable Mg-Al layered double hydroxide supported cobalt phthalocyanine catalyst, *Fuel Process. Technol.*, 2017, **162**, 135–146.

11 D. Chauhan, *et al.*, Photo-assisted oxidation of thiols to disulfides using cobalt "Nanorust" under visible light, *New J. Chem.*, 2015, **39**(8), 6193–6200.

12 M. S. Nazir, *et al.*, A Review on the Methods in Diesel Desulfurization, *Curr. Anal. Chem.*, 2021, **17**(6), 815–830.

13 T. A. Saleh and I. M. Abdullahi, Advances in Nanocatalyzed Hydrodesulfurization of Gasoline and Diesel Fuels, in *Nanotechnology in Oil and Gas Industries: Principles and Applications*, ed. T. A. Saleh, Springer International Publishing, Cham, 2018, pp. 67–96.

14 A. Singh, *et al.*, Syntheses, design strategies, and photocatalytic charge dynamics of metal–organic frameworks (MOFs): a catalyzed photo-degradation approach towards organic dyes, *Catal. Sci. Technol.*, 2021, **11**(12), 3946–3989.

15 V. Chandra Srivastava, An evaluation of desulfurization technologies for sulfur removal from liquid fuels, *RSC Adv.*, 2012, **2**(3), 759–783.

16 F. Boshagh, M. Rahmani and W. Zhu, Recent Advances and Challenges in Developing Technological Methods Assisting Oxidative Desulfurization of Liquid Fuels: A Review, *Energy Fuels*, 2022, **36**(21), 12961–12985.

17 A. M. Matloob, D. R. Abd Elhafiz and D. Abol-Fotouh, Low temperature coupled oxidative/adsorptive desulfurization catalyzed by FeOOH/rGO nanocomposite, in *The International Conference on Chemical and Environmental Engineering*, Military Technical College, 2024.

18 A. M. Matloob, *et al.*, Hybrid Nanoarchitectonics with Cr, Fe-MOF/Graphene Nanocomposite for Removal of Organic Sulfur Compounds from Diesel Fuel, *J. Inorg. Organomet. Polym. Mater.*, 2023, **33**(1), 254–265.

19 A. Riaz, *et al.*, Development of reduced graphene oxide-supported novel hybrid nanomaterials (Bi_2WO_6@rGO and Cu-WO_4@rGO) for green and efficient oxidative desulfurization of model fuel oil for environmental depollution, *Environ. Res.*, 2022, **212**, 113160.

20 H. M. Salem, *et al.*, Enhancing ultrasound-assisted oxidative desulfurization of fuels using hierarchical metal–organic framework and ordered mesoporous silica composite, *J. Chem. Technol. Biotechnol.*, 2025, **100**(8), 1667–1678.

21 R. M. A. Mahmoud, *et al.*, Sonochemical synthesis of heterostructured ZnO/Bi_2O_3 for photocatalytic desulfurization, *Sci. Rep.*, 2023, **13**(1), 19391.

22 M. Radko, *et al.*, Catalytic and photocatalytic oxidation of diphenyl sulphide to diphenyl sulfoxide over titanium dioxide doped with vanadium, zinc, and tin, *RSC Adv.*, 2020, **10**(7), 4023–4031.

23 S. A. Shah, *et al.*, Sustainable oxidative desulfurization of fuel via lignin-derived heterogeneous catalysis: Optimized by Box-Behnken design for high efficiency under mild conditions, *Int. J. Biol. Macromol.*, 2025, **310**, 143404.

24 Q. Liang, *et al.*, Sulfur-doped graphitic carbon nitride decorated with zinc phthalocyanines towards highly stable and efficient photocatalysis, *Appl. Catal., A*, 2016, **519**, 107–115.

25 W. Zhao, *et al.*, A critical review on surface-modified nano-catalyst application for the photocatalytic degradation of volatile organic compounds, *Environ. Sci.: Nano*, 2022, **9**(1), 61–80.

26 J.-Y. Li, *et al.*, Selective Organic Transformations over Cadmium Sulfide-Based Photocatalysts, *ACS Catal.*, 2020, **10**(11), 6262–6280.

27 S. S. Priya and R. Khatri, Recent Advances on Catalysts Based on MoS_2: A Review on Diverse Applications, *ChemistrySelect*, 2025, **10**(19), e202405247.

28 Y. Gupta, *et al.*, Molybdenum Chalcogenides for Photo-Oxidative Desulfurization of Liquid Fuels Under Ambient Conditions: Process Optimization, Kinetics, and Recyclability Studies, *Catal. Lett.*, 2023, **153**(3), 643–658.

29 J. Cui, *et al.*, Synthesis $BiVO_4$ modified by CuO supported onto bentonite for molecular oxygen photocatalytic oxidative desulfurization of fuel under visible light, *Fuel*, 2021, **290**, 120066.

30 O. Monfort and G. Plesch, Bismuth vanadate-based semiconductor photocatalysts: a short critical review on the efficiency and the mechanism of photodegradation of organic pollutants, *Environ. Sci. Pollut. Res.*, 2018, **25**(20), 19362–19379.

31 X. Zhang, *et al.*, A review on WO_3-based composite photocatalysts: synthesis, catalytic mechanism and diversified applications, *Rare Met.*, 2024, **43**(8), 3441–3459.

32 J. Cai, *et al.*, Activation of MoS_2 via tungsten doping for efficient photocatalytic oxidation of gaseous mercury, *Appl. Catal., B*, 2022, **314**, 121486.

33 P. Kalita, *et al.*, A critical review on emerging photoactive porous materials for sulfide oxidation and sulfur mustard decontamination, *Green Chem.*, 2023, **25**(15), 5789–5812.

34 M. Bagheri, M. Y. Masoomi and A. Morsali, A MoO_3–Metal–Organic Framework Composite as a Simultaneous Photocatalyst and Catalyst in the PODS Process of Light Oil, *ACS Catal.*, 2017, **7**(10), 6949–6956.

35 B. N. Bhadra, *et al.*, TiO_2-Containing Carbon Derived from a Metal–Organic Framework Composite: A Highly Active Catalyst for Oxidative Desulfurization, *ACS Appl. Mater. Interfaces*, 2017, **9**(36), 31192–31202.

36 A. Fujishima and K. Honda, Electrochemical Photolysis of Water at a Semiconductor Electrode, *Nature*, 1972, **238**(5358), 37–38.

37 X. Chen and S. S. Mao, Titanium Dioxide Nanomaterials: Synthesis, Properties, Modifications, and Applications, *Chem. Rev.*, 2007, **107**(7), 2891–2959.

38 M. Pawar, S. Topcu Sendoğdular and P. Gouma, A Brief Overview of TiO_2 Photocatalyst for Organic Dye Remediation: Case Study of Reaction Mechanisms Involved in Ce-TiO_2 Photocatalysts System, *J. Nanomater.*, 2018, **2018**(1), 5953609.

39 V. Etacheri, *et al.*, Visible-light activation of TiO_2 photocatalysts: Advances in theory and experiments, *J. Photochem. Photobiol., C*, 2015, **25**, 1–29.

40 H. Khan, *et al.*, Spray dried TiO_2/WO_3 heterostructure for photocatalytic applications with residual activity in the dark, *Appl. Catal., B*, 2018, **226**, 311–323.

41 G. P. Lepore, L. Persaud and C. H. Langford, Supporting titanium dioxide photocatalysts on silica gel and hydrophobically modified silica gel, *J. Photochem. Photobiol., A*, 1996, **98**(1), 103–111.

42 Y. Tang, *et al.*, Magnetic TiO_2-graphene composite as a high-performance and recyclable platform for efficient photocatalytic removal of herbicides from water, *J. Hazard. Mater.*, 2013, **252–253**, 115–122.

43 J. Melcher, *et al.*, Influence of TiO_2 agglomerate and aggregate sizes on photocatalytic activity, *J. Mater. Sci.*, 2017, **52**(2), 1047–1056.

44 J. C. Yu, *et al.*, Efficient Visible-Light-Induced Photocatalytic Disinfection on Sulfur-Doped Nanocrystalline Titania, *Environ. Sci. Technol.*, 2005, **39**(4), 1175–1179.

45 K. Nagaraj, *et al.*, Photocatalytic advancements and applications of titanium dioxide (TiO_2): Progress in biomedical, environmental, and energy sustainability, *Next Res.*, 2025, **2**(1), 100180.

46 A. B. Djurišić, Y. He and A. M. C. Ng, Visible-light photocatalysts: Prospects and challenges, *APL Mater.*, 2020, **8**(3), 030903.

47 G. Iervolino, *et al.*, Limitations and Prospects for Wastewater Treatment by UV and Visible-Light-Active Heterogeneous Photocatalysis: A Critical Review, in *Heterogeneous Photocatalysis: Recent Advances*, ed. M. J. Muñoz-Batista, A. Navarrete Muñoz and R. Luque, Springer International Publishing, Cham, 2020, pp. 225–264.

48 B. A. Bhanvase, T. P. Shende and S. H. Sonawane, A review on graphene–TiO_2 and doped graphene–TiO_2 nanocomposite photocatalyst for water and wastewater treatment, *Environ. Technol. Rev.*, 2017, **6**(1), 1–14.

49 M. Minella, F. Sordello and C. Minero, Photocatalytic process in TiO_2/graphene hybrid materials. Evidence of charge separation by electron transfer from reduced graphene oxide to TiO_2, *Catal. Today*, 2017, **281**, 29–37.

50 A. Eshaghi and H. Moradi, Optical and photocatalytic properties of the Fe-doped TiO_2 nanoparticles loaded on the activated carbon, *Adv. Powder Technol.*, 2018, **29**(8), 1879–1885.

51 A. M. Matloob, *et al.*, Metal organic framework-graphene nano-composites for high adsorption removal of DBT as hazard material in liquid fuel, *J. Hazard. Mater.*, 2019, **373**, 447–458.

52 H. M. Abd El Salam and A. S. Morshedy, TiO_2@Metal organic framework $Ni_2(BDC)_2(DABCO)$ as an efficient water splitting heterogeneous photocatalyst for enhanced green hydrogen generation under visible light, *Int. J. Hydrogen Energy*, 2025, **151**, 150142.

53 J. Meng, *et al.*, Highly Efficient Visible-Light Photocatalysts: Bi_2O_3@TiO_2 Derived from Ti-MOFs for Eriochrome Black T Degradation: A Joint Experimental and Computational Study, *Catalysts*, 2024, **14**, 829.

54 A. S. Morshedy, *et al.*, The production of clean diesel fuel by facile sun light photocatalytic desulfurization process using Cd-based diacetate as a novel liquid photocatalyst, *J. Cleaner Prod.*, 2021, **279**, 123629.

55 S. I. Hassan, *et al.*, Solvent extraction of oxidized diesel fuel: Phase equilibrium, *Fuel Process. Technol.*, 2013, **106**, 127–132.

56 L. Li, *et al.*, Titanium-Based MOF Materials: From Crystal Engineering to Photocatalysis, *Small Methods*, 2020, **4**(12), 2000486.

57 R. Bibi, *et al.*, Synthesis of Amino-Functionalized Ti-MOF Derived Yolk–Shell and Hollow Heterostructures for Enhanced Photocatalytic Hydrogen Production under Visible Light, *ACS Sustain. Chem. Eng.*, 2019, **7**(5), 4868–4877.

58 L. Feng, *et al.*, Catalytic Porphyrin Framework Compounds, *Trends Chem.*, 2020, **2**(6), 555–568.

59 R. Hengerer, *et al.*, Structure and stability of the anatase TiO_2(101) and (001) surfaces, *Surf. Sci.*, 2000, **460**(1), 162–169.

60 S. Chen, *et al.*, Synthesis of black TiO_2 with efficient visible-light photocatalytic activity by ultraviolet light irradiation and low temperature annealing, *Mater. Res. Bull.*, 2018, **98**, 280–287.

61 M. Haghighi, *et al.*, Reduced graphene oxide supported Ti-based metal–organic framework as a novel electrochemical sensor for electro-oxidation of Propranolol, *J. Mater. Sci.: Mater. Electron.*, 2021, **32**(7), 8396–8409.

62 A. M. Matloob and S. Said, Hybridizing silica and $Cu_3(BTC)_2$ to synthesize copper containing catalysts for ethanol conversion, *J. Mol. Liq.*, 2024, **406**, 125062.

63 C. E. Zubieta, P. V. Messina and P. C. Schulz, Photocatalytic degradation of acridine dyes using anatase and rutile TiO_2, *J. Environ. Manage.*, 2012, **101**, 1–6.

64 F. Liu, *et al.*, Porphyrin-based MOFs for photocatalysis in water: advancements in solar fuels generation and pollutants degradation, *Inorg. Chem. Front.*, 2024, **11**(8), 2212–2245.

65 Z. Wang and H. Einaga, WO_3-based Materials for Photocatalytic and Photoelectrocatalytic Selective Oxidation Reactions, *ChemCatChem*, 2023, **15**(21), e202300723.

66 X. Chen, *et al.*, Increasing Solar Absorption for Photocatalysis with Black Hydrogenated Titanium Dioxide Nanocrystals, *Science*, 2011, **331**(6018), 746–750.

67 W. Han, Z. Tang and Q. Lin, Morphology-Controlled Synthesis of the Metal–Organic Framework-Derived Nanorod Interweaved Lamellose Structure Co_3O_4 for Outstanding Catalytic Combustion Performance, *Cryst. Growth Des.*, 2019, **19**(8), 4546–4556.

68 X. Bai, *et al.*, MOF-derived porous TiO_2 decorated with n-type Cu_2O for efficient photocatalytic H_2 evolution, *New J. Chem.*, 2021, **45**(37), 17332–17338.

69 A. S. Morshedy, *et al.*, Solar-powered commercial diesel fuel desulfurization: Exploring the factors affecting and recyclability of mesoporous Tl-doped TiO_2 nanofiber photocatalysts, *J. Cleaner Prod.*, 2024, **449**, 141713.

70 H. M. El Sharkawy, M. A. Abo El-Khair and A. S. Morshedy, Construction of SnS_2@SnO_2 nanocomposite Z-scheme heterojunction for dual-functional photocatalysis: Green hydrogen generation and crystal violet degradation, *Int. J. Hydrogen Energy*, 2025, **137**, 471–486.

71 A. S. Morshedy, *et al.*, Highly efficient Imprinted Polymer Nanocomposites for photocatalytic desulfurization of real diesel fuel, *Environ. Technol. Innovation*, 2021, **21**, 101206.

72 U. A. Metwally, *et al.*, Poly N-(2-aminoethyl) acrylamide-NiO composite as novel efficient photocatalyst for desulfurization of diesel fuel under visible-light irradiation, *Egypt. J. Chem.*, 2021, **64**(10), 3–4.

73 M. Barmala, M. Behnood and M. R. Omidkhah, Photo oxidation of DBT using carbon nanotube titania composite as visible light active photo catalyst, *J. Cent. South Univ. (Engl. Ed.)*, 2018, **25**(7), 1642–1650.

74 S. Arunmetha, *et al.*, Preparation of sulfur doped TiO_2 nanoparticles from rutile sand and their performance testing in hybrid solar cells, *J. Mater. Sci.: Mater. Electron.*, 2021, **32**(24), 28382–28393.

75 C. Di Valentin, G. Pacchioni and A. Selloni, Reduced and n-Type Doped TiO_2: Nature of Ti^{3+} Species, *J. Phys. Chem. C*, 2009, **113**(48), 20543–20552.

76 C. Liu, *et al.*, Crystal facet-dependent p-type and n-type sensing responses of TiO_2 nanocrystals, *Sens. Actuators, B*, 2018, **263**, 557–567.

77 H. Li, *et al.*, State-of-the-Art Progress in Diverse Heterostructured Photocatalysts toward Promoting Photocatalytic Performance, *Adv. Funct. Mater.*, 2015, **25**(7), 998–1013.

78 B. B. Shaik, *et al.*, Titanium Dioxide/Graphene-Based Nanocomposites as Photocatalyst for Environmental Applications: A Review, *ChemistrySelect*, 2024, **9**(46), e202403521.

79 J. Xu, *et al.*, Enhanced desulfurization performance of model fuel by Cu–ZnO/TiO_2 heterostructure, *RSC Adv.*, 2024, **14**(49), 36733–36744.

80 X. N. Pham, *et al.*, Highly efficient photocatalytic oxidative desulfurization of dibenzothiophene with sunlight irradiation using green catalyst of Ag@AgBr/Al-SBA-15 derived from natural halloysite, *J. Ind. Eng. Chem.*, 2020, **90**, 358–370.

81 P. Jabbari, *et al.*, Synthesis of Cu-doped TiO_2 modified $BiVO_4$ for photocatalytic oxidative desulfurization (PODS) of a model fuel, *J. Photochem. Photobiol., A*, 2024, **452**, 115625.

82 B. Moeinifard and A. Najafi Chermahini, Fabrication of Au-doped mesoporous TiO_2 supported on g-C_3N_4 as an efficient light-assisted catalyst for oxidative desulfurization of model fuels with different sulfur content, *J. Mater. Sci.: Mater. Eng.*, 2025, **20**(1), 14.

83 F. Wu, *et al.*, Oxidative desulfurization catalyzed by magnetically recoverable $CoFe_2O_4$ nano-particles, *Arabian J. Chem.*, 2025, **18**(1), 106076.

84 A. Tiple, P. S. Sinhmar and P. R. Gogate, Improved direct synthesis of TiO_2 catalyst using sonication and its application for the desulfurization of thiophene, *Ultrason. Sonochem.*, 2021, **73**, 105547.

85 W. Zhu, *et al.*, Photocatalytic oxidative desulfurization of dibenzothiophene catalyzed by amorphous TiO_2 in ionic liquid, *Korean J. Chem. Eng.*, 2014, **31**(2), 211–217.

86 A. Anggraini, J. Jefri and A. Lesbani, Efficient Desulfurization of 4-Methyldibenzothiophene Using $H_5PV_2Mo_{10}O_{40}/TiO_2$: A Catalytic Approach, *Indones. J. Mater. Res.*, 2025, 3(1), 17–23.

87 Z. Song, *et al.*, Synthesis of TiO_2-Modified Y Zeolite and its Adsorption-Catalytic Oxidative Desulfurization Performance, *Silicon*, 2024, **16**(10), 4159–4172.

88 M. Abdollahi, *et al.*, Photocatalytic oxidative desulfurization of model fuel over visible light-active Cu-impregnated carbon-doped TiO_2, *J. Cleaner Prod.*, 2022, **380**, 134968.

89 X.-j. Wang, *et al.*, Preparation of TiO_2 in Ionic Liquid via Microwave Radiation and in Situ Photocatalytic Oxidative Desulfurization of Diesel Oil, *Energy Fuels*, 2012, **26**(11), 6777–6782.